The free gas zone beneath gas hydrate bearing sediments and its link to fluid flow: 3-D seismic imaging offshore mid-Norway

Andreia Plaza-Faverola, Stefan Bünz and Jürgen Mienert

Department of Geology, Dramsveien 201, University of Tromsø, Norway

Abstract

Hydrate recycling and vertical migration of fluids from deep sources are processes evoked as controllers of the formation and stability of the free gas zone (FGZ) beneath the base of the gas hydrate stability zone (BGHSZ). These processes have been often investigated through analytical and numerical modeling at some locations in continental margins. However, the seismic response of sediments deformed by such mechanisms has been poorly investigated due to the lack of reliable seismic resolution to clearly image anomalies confined to the FGZ. The present study is dedicated to the seismic characterization of the FGZ beneath the BGHSZ at a hydrate site in Nyegga using high resolution P-Cable 3D seismic data. Dim amplitude anomalies, showing mainly lineations in a polygonal pattern of distribution, 50-80 m vertical extension, 150-300 m lateral extension and up to a few kilometers long, are interpreted as evidence of sediment remobilization possible aided by hydrate dissociation at focused fluid flow zones beneath BGHSZs. The exclusive occurrence of the anomalies within a depth range comprising estimated paleo BGHSZs during the last 160 ka, suggests that the anomalies are associated to paleo-hydrate bearing sediment seals emplaced at depths controlled by overburden. Polygonal faulting, sediment overburden and sufficient sourced gas from depth are major settings controlling the migration of hydrocarbon to shallow reservoirs and to the seafloor in Nyegga.

1. Introduction

Gas hydrate distributions in mid-Norwegian margin sediments are commonly inferred from the occurrence of a bottom-simulating reflector (BSR) that lies at the predicted base of the gas hydrate stability zone (BGHSZ) (Bünz et al., 2003). Its geophysical detection is possible due to the low seismic velocity of the free gas zone (FGZ) directly beneath the BGHSZ. The FGZ varies in thickness but is generally less than 100 meters thick (e.g. Bünz et al., 2005). Several authors have shown that the FGZ sustains the formation of gas hydrates (Hornbach et al., 2004; Haacke et al., 2009; Haacke et al., 2007; Liu and Flemings, 2007).

There is a consensus that mounds and pockmarks observed at the seabed on many passive continental margins form primarily as a consequence of fluid venting induced by excess pore pressure (e.g. Cathles et al., 2010; Hustoft et al., 2010; Judd and Hovland, 2007; Løseth et al., 2009; Tjelta et al., 2007). In Nyegga, offshore Norway, the presence and extension of the FGZ beneath the GHSZ have been assessed at several locations through seismic velocity modeling (Bouriak et al., 2000; Bünz et al., 2005; Mienert et al., 2005b; Plaza-Faverola et al., 2010a; Westbrook et al., 2008a). However, the dynamics of the free gas and the evolution of the FGZ are only poorly understood. Amongst the key questions are, the origin of the gas-charged fluids, free-gas accumulation mechanisms or the effect of excess pore pressure on the sediments.

Commonly, the lack of sub-seafloor imaging resolution hinders the detailed seismic geomorphological analysis and comprehension of mechanisms by which sediments within the gas layer beneath the BGHSZ are affected. Apart from observed dim amplitude anomalies inside gas chimneys (e.g. Løseth et al., 2009) and observed chaotic reflections beneath the BSRs (e.g. Westbrook et al., 2008b), seismic anomalies helping to elucidate the processes characterizing the FGZ beneath the GHSZ have been rarely reported (Bünz and Mienert, 2004). Dim amplitude anomalies have been described as areas in the seismic section where reflections from stratigraphic levels are visible but weaker in relation to adjacent areas and where reflection continuity and amplitudes are reduced (Løseth et al., 2003). The resolution of the 3D P-Cable data (Petersen et al., 2010) available for this study allows for an exceptional imaging of dim amplitude anomalies at the FGZ in Nyegga. It offers the opportunity to investigate free-gas dynamics, the interaction with the upward-moving hydrate-gas interface and the mechanical response of the host sediments.

This study integrates shallow high-resolution 3D with deeper lower resolution 3D seismic data in the Nyegga area to report: (1) how sediments within the FGZ beneath the GHSZ are affected by the upward migration of buoyant fluids and possibly by the dissociation of gas hydrates, and (2) the relation between chimney distributions, underlying fluid escape related deformations and deep faulting.

2. Geological and geophysical background

The research concentrated on the northern part of the Nyegga region located between $4^o48'-5^o30'$ longitude and $64^o36'-4^o48'$ latitude at the mid-Norwegian continental margin (figure 1). Nyegga is bounded by the Trøndelag platform to the east, Vøring plateau to the north, Møre basin to the south and by the Jan Mayen transform zone to the west (Brekke, 2000). Specifically, this study focuses at the maximum uplift region of the Helland Hansen arch (HHA) (figure 2) and northern flank of the Storegga slide escarpment (figure 2). The Helland Hansen arch is one of the large-scale domes formed along the margin during Eocene-Miocene inversion tectonics after the continental breakup (Gómez and Vergés, 2005; Lundin and Doré, 2002). The northern and eastern flanks of the arch structure were accentuated most likely during the last 10 Ma due to differential compaction induced by thick prograding sedimentary wedges (Gómez and Vergés, 2005; Kjeldstad et al., 2003). The inversion is not only expressed as elongated dome anticlines along the margin but also as discrete structures clearly recognized as compressional reactivation of older normal faults (Hansen et al., 2005).

The concerned stratigraphic formations for the present study include from bottom to top: the Lower Eocene-Lower Miocene Brygge Formation, the Miocene to Upper Pliocene Kai Formation and the Plio-Pleistocene Naust Formation (Dalland et al., 1988). The Brygge Formation consists mainly of claystone with biogenic ooze and interbeds of sandstones (Dalland et al., 1988; Hansen et al., 2005). Large evacuation craters, eroding up to 200 m into the ooze sediments of the Brygge Formation, exist at the shallower crest of the HHA (Riis et al., 2005). The Kai Formation consists of alternating claystone, siltstone and sandstone with limestone interbeds (Hansen et al., 2005). It represents predominantly deep-water basinal sedimentation onlapping the Paleogene domes (Bryn et al., 2005).

The Naust Formation resulted from glacial-interglacial fluctuations in sediment distribution and accumulation (Berg et al., 2005; Hjelstuen et al., 1999; Nygård et al., 2005; Rise et al., 2006). It consists of thick accumulations of debris flow deposits interbedded with hemipelagic and contouritic sediments (Bryn et al., 2005). The suggested age of the Naust Formation is 2.8-0 Ma (Rise et al.,

2006). The site studied here does not cover the thickest glacial debris flow deposits (figure 2). Fluid reservoirs, gas chimneys and gas hydrate systems are therefore confined to mainly fine grained marine and glacial marine clay sequences (Berg et al., 2005). During deposition of Naust the sedimentation rate increased significantly if compared to the Eocene-Pliocene Brygge and Kai formations and as a result the continental shelf prograded up to 200 km westward (Eidvin et al., 2000; Rise et al., 2006). Table 1 provides a chronological synthesis of Cenozoic geological processes along the Mid Norwegian margin found in the literature.

Bottom water current activity has influenced sedimentation patterns along the margin since mid-Miocene time. As a result, large contourite drifts deposited during interglacial cycles. These drift deposits represent accumulation periods of approximately 100 ka (Bryn et al., 2005; Stoker et al., 2005). The contouritic infills appear as extensive homogenous layers with more brittle and low shear strength sediments if compared to the glacial deposits (Bryn et al., 2005; Leynaud et al., 2009).

At several locations along the Norwegian margin vertical zones of seismic chaotic reflections below the BGHSZ are interpreted as paths for fluid migration from deeper sources, e.g. from Paleogene reservoirs (Bünz and Mienert, 2004; Hansen et al., 2005; Hustoft et al., 2007; Løseth et al., 2009; Plaza-Faverola et al., 2010a). Prolific Jurassic source rocks and Cretaceous-Paleocene-Eocene hydrocarbon reservoirs are reported from the Vøring and Møre basins (Brekke et al., 1999; Spencer et al., 1999). In addition, remobilization of the ooze sediments at the shallower crest of the HHA is also evidence of fluid migration from deep reservoirs in the region. The rapid deposition of large amounts of Naust sediments during the last 400 ka is thought to have caused large excess pore pressure at the crest of the arc where upward migrating fluids accumulated (Rise et al., 2006).

Polygonal fault development affected the fine-grained, hemi-pelagic sediments of the Kai (Berndt et al., 2003) and lower Naust Formations (Gay and Berndt, 2007) as well as the upper Brygge formation (Hansen et al., 2005). It has been associated with active fluid flow in the region since Miocene times (Berndt et al., 2003). The polygonal faults are thought to play a major role connecting deeper and shallow reservoirs (Berndt et al., 2003; Bünz and Mienert, 2004; Gay and Berndt, 2007). Within the lower Naust unit a major level for fluid accumulation has been well defined by velocity analysis showing a low velocity layer in the Vøring basin (Reemst et al., 1996), the Ormen Lange area (Mienert et al., 2005a), the western Nyegga area (Bünz et al., 2005; Westbrook et al., 2008a) and within Nyegga itself (Plaza-Faverola et al., 2010a). Beneath the present-day BGHSZ, the FGZ

shows high amplitudes at the top of the zone and low P-wave velocities (e.g. (Bünz et al., 2005; Plaza-Faverola et al., 2010a; Westbrook et al., 2008a).

Modelling of the GHSZ dynamics in the Storegga slide region has shown that the hydrate formation and dissociation behaves dynamically. It results in decreases or increases of the GHSZ that is controlled by changing natural conditions such as bottom water temperature, geothermal gradient, sea-level, sedimentation rate and subsidence rates (Mienert et al., 2000; Mienert et al., 1998; Vanneste and Mienert, 2005). According to Vanneste and Mienert, (2005) the hydrate stability zone had an asymmetric evolution with time and with depth. The effect of temperature changes on the hydrate stability is more pronounced above 800 m water depth while sea level has a dominant effect in the deeper water areas of the margin where ocean water temperature changes are only minor (Vanneste and Mienert, 2005).

The present-day seafloor within the Nyegga region is particularly interesting due to an extensive mounds and pockmark field where micro seepage of methane (Hovland et al., 2005; Mazzini et al., 2006; Paull et al., 2008; Vaular et al., 2010) and shallow gas hydrates (Ivanov et al., 2007; Vaular et al., 2010) have been sampled at different localities. Some of the chimneys related to pockmarks have also been investigated through high resolution seismic velocity experiments suggesting the occurrence of high velocity material, most likely gas hydrate at the interior of the chimneys (Jose et al., 2008; Plaza-Faverola et al., 2010b).

Table 1 provides a chronological summary of major geological events in the region based on publications. Relevant features of the geological setting comprising the Nyegga region are compiled in a regional seismic profile (figure 2).

3. Data and methods

The present study is based on the integration of 2D and 3D seismic data of different resolution and depth coverage (table 2). A high-resolution 3D seismic data set (P-Cable 3D) covers an area of approximately 3x10 km towards the north of Nyegga (figure 1). It provides the base for a detailed investigation of features within the FGZ beneath the GHSZ. This data set was acquired in the summer 2008 on board R/V Jan Mayen, from the University of Tromsø (Bünz et al., 2008). A second 3D seismic data set (ST0408) of lower resolution but with deeper penetration (table 2), provided by Statoil, was used to determine the effect of faults and deep structures on the distribution of gas chimneys and dim amplitude anomalies within the shallower strata. Although in less detail, dim

amplitude anomalies at the FGZ are also observed in the ST0408 data set. It is therefore unlikely that the investigated dim amplitude anomalies are seismic artifacts. 2D regional lines were used to show the overall geological settings and major stratigraphic units to describe what may control fluid flow in the region (figure 2, table 1).

The present study has a mainly descriptive character for which the methodology can be summarized in four steps:

Integrating geological and geophysical observations to get a regional overview of fluid flow related features integrated in the geological context of the region. Major depositional features such as stratigraphic units, clinoforms of glacigenic debris flow deposits, hemipelagic glacio-marine sediment deposits, contour current deposits, gas rich layers, deep routed chimneys, and chaotic strata, were interpreted along a north-south 2D regional profile (figure 2, table 1).

Mapping consecutive seismic horizons within the GHSZ and FGZ to search for the vertical extension of fluid escape related features. 3D seismic data allowed to determine the 3D geometry and spatial distribution of seismic anomalies that represent permanent changes within the sediment column induced by fluid escape that often cannot be identified through other than indirect methods (Løseth et al., 2009).

Four main seismic horizons within the sedimentary column between the seafloor and top of the Brygge formation were mapped in the high-resolution P-Cable 3D data set for the investigation of chimney distribution and underlying dim amplitude anomalies at the FGZ beneath the BGHSZ. Structural attribute maps (i.e. variance) were used to get dimensions and spatial distribution of fluid-escape features appearing at the shallower gas reservoir as well as for characterization of faults.

The attribute of variance implemented, searches for lateral amplitude discontinuities and make them look like isolated edges (Van Bemmel and Pepper, 2000). The attribute can be used to enhance faults and stratigraphical features characterized by lateral amplitude anomalies. The normalized variance

algorithm is computed as: $\sigma^2(t) = \dfrac{\sum_{j=t-\frac{L}{2}}^{j=t+\frac{L}{2}} w_{j-t} \sum_{i=1}^{I}(x_{ij}-x_j)^2}{\sum_{j=t-\frac{L}{2}}^{j=t+\frac{L}{2}} w_{j-t} \sum_{i=1}^{I}(x_{ij})^2}$; where xij is the sample amplitude value

at a horizontal position i (i.e. trace number), and vertical position j; wj-t is the vertical smoothing term over a window of length L.

Analyzing the trend of faults and gas escape features at different sub-seafloor depths to search for a relationship between different observed fluid escape related features. Structural seismic attributes were calculated at the depth of consecutive reflectors between the present day base GHSZ and the mid-Brygge formation, using the ST0408 seismic data set. These maps were compared to structural maps of shallower reflectors in order to analyze the relation between the trend of shallow escape features and the trend of faults and deeper structures (figures 3, 4 and 5).

Modeling paleo-depths of BGHSZs (Appendix A) *to analyze to which extent fluid flow related features, currently observed within the FGZ, were within the GHSZ in the past.* Based on published sedimentation rates and interval P-wave velocities for the upper Naust S and T units depths of the BGHSZ at the time of deposition of H50 and INT reflectors were estimated. These are time periods inferred to be characterized by important fluid escape through chimneys of the Nyegga region (Plaza-Faverola et al., subm.).

4. Observations and results

4.1 Dim amplitude lineations in the FGZ beneath the BGHSZ

At Nyegga, dim amplitude zones are observable at layers beneath the BGHSZ (figures 3- 4). A gas-rich layer, approximately 60 m thick, occurs beneath the present-day BGHSZ. It is characterized by low P-wave velocities (Vp < 1500 m/s) (Bünz et al., 2005; Plaza-Faverola et al., 2010a; Westbrook et al., 2008a). The layer itself has a heterogeneous seismic character (figure 3) due to a heterogeneous gas distribution (Bünz and Mienert, 2004). Chaotic reflections and dim amplitude zones are embedded in flat reflectors that interrupt against the conic shape of the anomalies (figure 4). The zones of dim anomalies are restricted to sediments that lie above the crest of the HHA (figure 2). In the vertical seismic cross-section the anomalies extend from the base of the high amplitude zone (HAZ) beneath the BGHSZ to approximately 80 m below it, where they terminate in nearly conical shapes (figures 3 and 4). At certain locations the anomalies connect to chimneys that continue towards the seafloor (figure 3).The seismic reflector at the shallower end of the anomalies is similar in seismic character to the reflector that coincides with the depths of the present day BGHSZ. It is a single-phase high amplitude reflector embedded in a low amplitude seismic sequence of approximately 10 m thickness (figure 3). The reflector seems to indicate the presence of a broken seal (figure 3). The dim amplitude anomalies terminate against this laterally interrupted reflector although some of the dimming zones reappear above it giving the overlying sequence a chaotic seismic character (figure 3). Sediments at lower Naust and deeper formations are characterized by

seismic blanking underlying the region with dim amplitude anomalies in upper Naust (figure 2 and 3).

Reflectors beneath the base of the dim amplitude anomalies are continuous but upwardly bended (figure 3 and 4). The upwardly bended reflection zones generally coincide with the junction of polygonal faults with opposite dip (figure 3 and 4).

The variance seismic attribute enhances faults and other structural features characterized by amplitude lateral anomalies (Van Bemmel and Pepper, 2000). In the variance map the zones of chaotic, dim amplitude anomalies within the present day gas rich layer appear as parallel and orthogonal elongated features of ca. 300 m thickness mainly NNE-SSW oriented (figure 5). Also zones of isolated circular anomalies with diameters up to a few hundred of meters occur (figure 4).

4.2 Faults and inversion structures at lower Naust and deeper

Four consecutive variance maps were calculated for horizons between the top of the gas layer beneath the present day BGHSZ and the top of Brygge formation. Depths of the variance maps are approximately 270, 340, 430 and 590 mbsf respectively (interval velocities from Plaza-Faverola et al., 2010b). The maps show that different structural features are dominant at different depths within lower Naust sediments (figure 6). The variance map at the base of the high reflectivity zone beneath the GHSZ (figure 6-A) is characterized by randomly distributed iceberg-scour features that impede the ease recognition of faults. At a horizon within the shallow gas layer beneath the present day GHSZ (figure 6-B) the dominant structures are linear and elliptical dim amplitude anomalies. At this depth faults are in general recognized crossing circular to elliptical anomalies. Elliptical anomalies are 250-300 m in diameter, associated to gas chimneys. Some of them terminate beneath the GHSZ but most of them bypass the seal towards the seafloor (figure 6).

The linear dim amplitude anomalies do not extend down towards the top of a deeper gas layer (Top Naust A). At this depth it is easier to recognize faults (figure 6-C). The elliptical anomalies appear narrower compared to the described horizons above (figure 6). Finally, sets of polygonal faults forming NNE-SSW linations characterize the top Brygge horizon (figure 6-D). Linear and elliptical dim amplitude anomalies do not appear at the top of Brygge (figure 6). Instead the imprint of the anomalies here is replaced by a clear imprint of polygonal faults (blue circles, figure 6-D).

The Brygge formation is highly faulted (Hansen et al., 2005). Upper Brygge sediments are characterized by a polygonal fault pattern consisting of linear sets that are NE-SW oriented (figure

6). Middle Brygge sediments are also characterized by a polygonal fault pattern but it consists of small cross-cutting faults forming tilted blocks of 400x700 m size in average, at the depth of the opal A/CT transition (figure 6, 7). Bright spots at the top of tilted blocks are recognized both in the vertical seismic profiles and in RMS amplitude maps where zones of anomalous high amplitudes are confined to the tops of some of the tilted blocks (figure 7-B). Composite, large, almost E-W trending faulted areas result from the connection of several small faults at the boundaries of the tilted blocks (figure 7-A).

A comparison of maps 6-D and 7-A suggests a propagation of the NNE-SSW oriented faults. However, the almost E-W oriented set of faults composed by the largest walls of the tilted blocks, at the depth of the opal A/CT transition, do not propagate towards the top of Brygge (figures 6, 7). This is an indication of different periods of deformation and fault formation. Tilted blocks, sometimes forming flower-like structures or small scale inversion folds (figure 6), with bright-spots at their tops (figure 7), may be indicators of gas trapping (figures 6, 7). These potential hydrocarbon traps presumably resulted from the Eocene-Miocene compression event (table 1), the same event responsible for the formation of the Helland Hansen Arch (e.g. Gómez and Vergés, 2005). Polygonal faults at the top of Brygge are posterior and as indicated by various authors are likely formed by hydraulic fracturing induced by sedimentary overload (Berndt et al., 2003; Bünz and Mienert, 2004; Gay and Berndt, 2007; Hustoft et al., 2007).

5. Interpretation and discussion

The Nyegga study area belongs to the Storegga gas-hydrate province (Bünz et al., 2003), a passive margin setting, which is characterized by a relatively steady but low flux system. Plaza-Faverola et al., (subm.) document that this system has been affected and disturbed by rapid sedimentation and ensuing generation of excess pore pressures in sub-surface sediments multiple times during the last 200 ka. Elevated pore pressures have led to a significant increase in fluid flux to the hydrate–phase boundary. The first of the major phases of fluid flux has probably led to the development of the Storegga gas-hydrate system emplacing an efficient permeability barrier that locally affected the accumulation of gas, the build-up of excess pore pressure, the remobilization of sediments and the formation of focused fluid-flow features. The interpretation and discussion of the results herein focuses on (1) the dynamic gas-hydrate and free-gas systems at the gas-hydrate phase boundary and (2) the distribution of fluid-escape features in the Nyegga area. This work provides new important

insights into dynamic processes of hydrate formation, hydrate dissociation, gas migration and their consequences for evolving gas-hydrate systems.

Mechanisms for the formation of anomalous seismic amplitude dimming zones

Seismic amplitude dimming has been previously attributed to the presence of gas (Løseth et al., 2009) or gas hydrates in sediments (Riedel et al., 2006) but the mechanisms causing such amplitude dimming as response to sediment deformation are not well understood (Løseth et al., 2009). Although in the studied Nyegga site dim amplitude lineations are at the inferred gas layer beneath the present day GHSZ, the sediments affected by dimming have been most likely within the GHSZ during the past (figure 8). The explanation of mechanisms for the formation of these anomalies needs to account for the conical shape (figure 4), the linear and polygonal distribution pattern (figure 5), their vertical extension (figure 4), the burial depth and the extension of the GHSZ for the time of their formation (figure 8).

The seismic character and conical shape of the dimming anomalies (figure 4) suggest that they represent permanent sediment deformation independently of whether or not these anomalous zones contain free gas at present. We focus our discussion on the assumption that they are in nature real deformational structures, though it is likely that being at present within the free gas layer, the anomalous zones contain gas. The dimensions of the observed dim amplitude features (50-80 m deep, 150-300 m thick and up to a few km long) exceed the dimensions of relict or modern iceberg-scour features described in the literature (e.g. Clark et al., 1989) or those observed in Nyegga (figure 5, 6) and adjacent regions in the mid Norwegian margin (e.g. Gay and Berndt, 2007; Hohbein and Cartwright, 2006). It is therefore unlikely that the observed dimming anomalies are related to iceberg scouring. We suggest that the dimming zones may be caused by one or a combination of two main processes: (1) sediment remobilization simply induced by buoyant fluids (i.e., gas) encountering a permeability barrier made of gas hydrate bearing sediments at a paleo-BGHSZ and/or (2) dissociation of gas hydrate at the hosting sediment-gas contact at focused fluid flow zones as the BGHSZ moved upwards while the sedimentary column built up.

Sediment remobilization caused by inverse density gradient

Fluid flow related features in seal-bypass systems (Cartwright et al., 2007) along continental margins have been associated to the vertical migration of buoyant fluids (e.g. Cartwright et al., 2007; Hovland and Judd, 1988; Judd and Hovland, 2007; Løseth et al., 2003) based on fluid migration

patterns in models of low density/viscosity material underlying higher density/viscosity material (Anketell et al., 1970). Inflow of water or gas, overpressure build-up due to critical sediment loading, and other external trigger forces can induce loss of intergranular contact and further liquefaction (Anketell et al., 1970). The deformational pattern of sediments caused by buoyant fluids will be dependent on the mobility of the material being deformed (Anketell et al., 1970 and references therein). Interestingly, it has been shown that in general the mobilization of material occurs along narrow pipe-like features distributed in a polygonal pattern, forming sags at the junctions between three polygons (e.g. figure 6 in Anketell et al., 1970).

Lineation pattern. The polygonal pattern in the vertical migration of buoyant material (Anketell et al., 1970) can be evoked to explain the polygonal pattern and lineations formed by the dim amplitude anomalies at the FGZ beneath the present day BGHSZ (figure 5-C). In a model of remobilization by buoyant fluids we expect hydrocarbons to have migrated, through faults and fractures, from a permeable layer within lower Naust units (Bünz et al., 2005; Plaza-Faverola et al., 2010a; Westbrook et al., 2008a) but also from deeper formations (i.e. Brygge), towards the FGZ beneath the GHSZ (figure 6, 7). Sediment remobilization would then be induced in zones where sediments locally reached excess of pore fluid saturations (figure 8).

Vertical extent and conical shape. The vertical extension of the observed anomalies, restricted to the present FGZ thickness, may have been controlled by the presence of permeability barriers, i.e. gas hydrate bearing sediments at paleo-bases of the GHSZ (figure 8). Buoyant fluids would migrate laterally beneath the permeability barrier promoting lateral spreading and flattening at the top of the deformational structure (Anketell et al., 1970). Experimental and field studies have also confirmed that in a system composed by a layer of fine-grained sediments over a layer of coarser sediments, gas accumulated in the courser sediment layer would migrate laterally within the sedimentary boundary before migrating vertically to the surface (Judd et al., 2002). This would explain the conical shape of the observed anomalies, flattening in its majority, against an inferred paleo-seal at c. 80 m beneath the present day BGHSZ in the study area (figure 3, 4, 8).

Nature of paleo-seals. The permeability barriers sealing the upcoming buoyant material were most likely conformed of gas hydrate bearing sediments immediately above paleo-bases of the GHSZ (figure 8).

Two major periods of fluid expulsion, in addition to the most recent post- LGM period (Hustoft et al., 2009), were suggested from approximately 160 and 130 ka (H50 and INT reflectors respectively) (Plaza-Faverola et al., subm.). We would therefore expect to see seismic anomalies related to sediment deformation responses due to gas supply or hydrate emplacement at the depth of the BGHSZ at these particular periods of time. Indeed, estimated depths of the BGHSZ at the time of deposition of INT and H50 reflectors match the vertical extension of the dim amplitude anomalies within the FGZ beneath the GHSZ (figure 9). For depths estimations we considered different rates of subsidence and GHSZ ocean temperature scenarios (appendix A, figure A-1)

In general the curves of hydrate stability show that a decrease of 0.5 C° in the bottom water temperature or a decrease of 2 C° in the geothermal gradient shifts the theoretical BGHSZ approximately 10 m downwards (figure A-1). Projecting the minimum and maximum calculated depths (figure A-1) at the time of deposition of INT and H50 shows that gas hydrate was likely to form within the sediments that appear remobilized, i.e. dim amplitudes anomalous zones, (figure 9). Indeed, the minimum depth of the BGHSZ calculated for the time of deposition of INT (curve "a" figure 9-A) and for H50 (curve "a" figure 9-B) fits the depth of the reflectors that we refer to as paleo-seals (figure 4, 8). The depth of the BGHSZ at the time of deposition of reflector H50 (figure A1, appendix A) is likely to have been the first efficient hydrate seal emplaced in the region (figure 8A-I and B-I, 9). During the first stage of hydrate emplacement in porous strata the permeability decreases fast reducing the hydraulic conductance locally in the GHSZ and fluid flux causing the thickening of the FGZ beneath the GHSZ (Nimblett and Ruppel, 2003).

Paleo-seals (i.e. gas hydrate-bearing layers) migrated to "relative" shallower depths as overburden caused hydrate-bearing sediments to pass down through the BGHSZ (e.g. Haacke et al., 2007), contributing with pore fluids and generation of excess pore pressure after dissociation, while a new and shallower gas hydrate seal above the new BGHSZ would form (figure 8A, 10). The seismic character of paleo-seals (figure 3) suggests that the stratigraphic level was preserved and that it was only locally bypassed (figure 3, 8).

Hydrate dissociation at the BGHSZ

In the previous model, based on sediment remobilization, we don't consider that sediment deformation response to gas hydrate dissociation itself can explain the dim-amplitude anomalies. However, that is an alternative scenario. In a simplified approach, continuous hydrate recycling

would be induced by continuous sedimentation (e.g. Haacke et al., 2008). Hydrate recycling is a common process affecting the zone immediately above and below the BGHSZ (Haacke et al., 2008; Kvenvolden and Barnard, 1983; Minshull and White, 1989). Hydrate emplaced in the sediment matrix is moved towards the BGHSZ (equivalent to upward migration of the BGHSZ) by different factors such as sedimentation rate, increase in geothermal gradient, and fall in sea level (appendix A). When hydrates pass below the BGHSZ it dissociate and produce free gas and water. If enough free gas is produced by hydrate dissociation the gas migrates again into the new GHSZ and re-forms hydrate (Kvenvolden and Barnard, 1983; Minshull and White, 1989). The source of gas at this stage of dissociation is however expected to be a mix between the gas continuously migrating upward from deep sources and the gas resulting from hydrate dissociation.

To account for the conical shape of the dim amplitude anomalies in a model of hydrate dissociation the lateral extension of the zone where hydrate dissociate, at each stage of recycling, has to increase towards shallower depths (figure 8B). To explain this increase in lateral extension we need to invoke again a focused fluid flow. Gas hydrate would have formed preferentially at sediment-upward migrating gas contacts above the BGHSZ. These contacts would in turn be broader at shallower depths, due to a similar processes of buoyancy and lateral migration beneath and along through impermeable interfaces (Anketell et al., 1970) as shown in figure 8A (sediment remobilization induced only by buoyant fluids). The volume of free gas increases towards the top of the FGZ and the immediately available free gas for recycling is confined to the few meters beneath the BGHSZ (Haacke et al., 2008). We infer a mechanism where part of the free gas migrates upward into the GHSZ to form more hydrate (recycling). Pore space left by dissociating gas hydrate may have rapidly been impinged by free gas inducing remobilization of the weakened sediments (figure 8B). The difference with the model in figure 8A resides mainly in that gas hydrate dissociation facilitated the remobilization mechanisms through weakening of the host sediments.

Similar coupling mechanisms of dissolution and sediment remobilization induced by focused fluid flow have been used to explain evaporite dissolution structures in the eastern Mediterranean (Bertoni and Cartwright, 2005). Indeed, although different materials (i.e. gas hydrate or evaporite) are involved in dissociation and dissolution processes respectively, both processes being induced by focused fluid flow, the seismic response to these mechanism are comparable (e.g. figure 9 in Bertoni and Cartwright, 2005; figure 8 in Cartwright et al., (2007)).

Seismic amplitude dimming structures are not observed elsewhere in the sedimentary column (figure 9). This suggests that an efficient hydrate seal was first emplaced at the approximate time of deposition of H50 reflector (~160 ka), for which the BGHSZ coincides with the base of the conical dim amplitude anomalies (figure 9). Estimated bases of the GHSZ for older paleo seafloors lie far beneath the base of the observed anomalies.

5.2 Fluid escape pathways from deep to shallow: polygonal faulting, polygonal amplitude dimming and chimney lineations

The distribution of seafloor fluid flow features in Nyegga is apparently random. Some authors concluded that orientation and distribution of faults can hardly explain the distribution of pockmarks in Nyegga (e.g. Hjelstuen et al., 2009). These conclusions are based on the lack of seismically resolvable evidence for the occurrence of faults and fractures within sediments where gas chimneys have passed through. Deep faulting has been however generally mentioned as a probable factor controlling the distribution of fluid flow features that show a certain lineation or polygonal pattern (Bünz et al., 2003; Gay and Berndt, 2007; Hustoft et al., 2007; Judd and Hovland, 2007; Judd et al., 2002; Pilcher and Argent, 2007).

It cannot be random that polygonal faults at the top of Brygge, polygonal dim amplitude anomalies beneath the BGHSZ and some linear groups of chimneys at shallow depths, have the same general orientation and show similar patterns of distribution (figure 5, 6). Remarkably, results from the field experiment in Torry Bay site, Scotland, by Judd et al., (2002) also showed that fluid seeps are not randomly distributed but rather arranged in linear groups possibly controlled by deeper faulting and by the nature of the upper sediment layers. The polygonal pattern of sediment remobilization described by Anketell et al., (1970) may be closely related with the pattern of polygonal faulting induced by sediment overburden. The observations presented in section 4 (figure 5) may support this hypothesis. Hydraulic polygonal faulting, inferred to be induced by overburden, is well documented in Nyegga and nearby (Berndt et al., 2003; Bünz et al., 2003; Gay and Berndt, 2007). Intuitively gas tended to migrate through certain weak zones within faults where permeability and fault morphology allowed the migration (e.g. Berndt, 2005) forming a not exactly, but nearly similar, polygonal pattern of sediment remobilization, i.e., seen as dim amplitude anomalies in the seismic.

The vertical extension of the dim-amplitude anomalies may indicate the time spam during which free gas accumulated beneath paleo-bases of the GHSZ before a first main period of fluid expulsion

towards the seafloor was triggered. The formation of "seal bypass systems" (Cartwright et al., 2007) must have been induced exclusively at locations where pore pressure exceeded lithostatic pressure within contacts between sediment and upwardly migrating gas (i.e. dim amplitude zones). Chimneys formed then at focused zones where pore pressure was locally increased or overburden pressure decreased (e.g. due to sediment loading or unloading between glacial periods) to the point of inducing vertical leakage (Pilcher and Argent, 2007). This explains the occurrence of chimneys at weak zones within the general orientation of faults and dim anomalies but not covering the complete extension of the projected fault plains or the complete extension of the dim amplitude anomalies (figure 5-A and B).

Isolated chimneys that are generally broader than the chimneys forming linear groups may have evolved at the junction of more than one underlying fault, as suggested by Gay et al. (2006) for some of the chimneys in the Congo basin. At Nyegga, one equally good example is the CNE03 chimney which seemingly forms at the junction between N-S and NE-SW trending elongated dim amplitude anomalies beneath the GHSZ (figure 5-C) that in turn may be related to the convergence of fluids from several opposite dipping polygonal faults at the top of Brygge (figure 5-D).

Potential hydrocarbon traps are inferred from high RMS values and phase reversal at the top of tilted blocks within Brygge and even at deeper inversion structures (figures 6, 7). Deep routed chimneys terminating at the BGHSZ provide evidence for the vertical migration of fluids from these potential deep gas traps in Brygge towards shallow gas reservoirs (figure 6, seismic profile). Polygonal faults of upper Brygge and lower Naust are likely major migration paths for upward migrating fluids. All these observations point towards a close relationship between the distribution of fluids deep in the sediment column and the distribution of chimneys in the shallower strata.

6. Conclusions

The high-resolution 3D seismic study characterises the free gas zone beneath the present day base gas hydrate stability zone in Nyegga offshore the mid-Norwegian continental margin. It records the occurrence of buried dim amplitude anomalies seemingly associated to mechanisms such as sediment remobilization induced by buoyant material and hydrate dissociation that provides evidence of sediment deformation response to focused fluid flow beneath the base of the gas hydrate stability zone.

The shape of the investigated anomalies suggests lateral migration of buoyant fluids against paleo-seals composed of gas hydrate bearing sediments. The exclusive occurrence of the anomalies within the approximately 80 m thick free gas zone beneath the gas hydrate stability zone comprises the estimated paleo-depths of the gas hydrate stability zone during the last 160 ka. This indicates that the anomalies are related to the relative upward movement of the base of the gas hydrate stability zone as the sedimentary column built-up. The depth of paleo-seals has therefore been mainly controlled by sedimentation rate and overburden. It is likely that an efficient hydrate-seal was first emplaced approximately 160 ka ago.

The polygonal and linear distribution of the anomalies following the main orientation trend of deep faults but not matching the exact fault extension or location suggests that faults drive fluids towards the free gas zone through an inhomogeneous mechanism where only segments of faults are active players. Similarly, the distribution of fluid escape chimneys is controlled by local excess pore pressure compared to lithostatic pressure at exclusive zones within the contacts between the sediments and upward migrating gas. Faults are therefore indirect controllers of chimney distributions in Nyegga.

Appendix A

Estimated depths of paleo BGHSZ

Theoretical depths of the BGHSZ at the period of deposition of reflectors H50 and INT (~125 and ~160 ka) are presented (figure 11) taking into account assumptions about eustatic sea-level changes (Dahlgren et al., 2002), sedimentary rates (Hjelstuen et al., 2005) or sedimentary thicknesses from Vp models (Plaza-Faverola et al., 2010b), subsidence rates (Dahlgren et al., 2002; Hjelstuen et al., 2005) and temperature (Mienert et al., 2000; Mienert and Posewang, 1999; Vanneste and Mienert, 2005). The local theoretical base GHSZ was calculated for the present day using the same assumptions and curves used by Plaza-Faverola et al., 2010b. The curves for hydrate stability are form Vanneste and Mienert (2005), and geothermal gradients from Mienert et al. (2000). The assumptions for the calculation of gas hydrate stability curves in the past are the following:

Compensation for eustatic sea level changes, subsidence and sedimentary rates are applied respect the current seafloor bathymetry. Seafloor depth at the location of CNE03 pockmark (~720 m) was taken as initial condition for the calculations (see figure 1 for location). A decrease of 100 m in the

sea-level respect the present day sea-level was considered as average for the period between 130-160 ka (Dahlgren et al., 2002).

The 160 and 130 ka ages are correlated to H50 and INT reflectors respectively (Berg et al., 2005; Hjelstuen et al., 2005; Rise et al., 2006); Plaza-Faverola et al., subm.). At the location of our investigation this time period corresponds to a sedimentary column of 80-120 m (according to the Vp model by Plaza-Faverola et al., 2010b). In average, 100 m of sediments need therefore to be removed from the present sedimentary column. Removing 100 m of sediments is equivalent to add up to the water column and we are therefore backed to a water depth of 720 m (same as the current water depth). We are basically assuming that during the last 160 ka the sedimentation rate was equivalent to sea-level rise.

Two subsidence rates are taken into account: 1.2 m/ka reported at the outer shelf, towards the Vøring basin (Dahlgren et al., 2002); and 0.3 m/ka reported slightly north of Nyegga (Hjelstuen et al., 2005). These rates represent approximately 150-190 m and 40-50 m of average subsidence during the last 130-160 ka. Averages values of 170 m and 45 m were taken respectively and compensated as subtraction to the water thickness getting two curves of hydrate stability at water-column thickness of 550 and 675 m respectively.

 Lacking information about water temperature changes before the LGM, water bottom temperature (WBT) were taken as -1C° corresponding to the LGM for water depths of 1000 m (Vanneste and Mienert, 2005) and -0.5 C° as measured at present at the CNE03 location (Nouzé and Fabri, 2007). Hydrate stability curves were estimated for both scenarios.

Geothermal gradient were taken as: 50 C°/km and 52 C°/km, e.g. representative for the mid-Norwegian margin (Vanneste and Mienert, 2005).

The curves were projected back in time at the two stratigraphic levels corresponding to 130 and 160 ka periods of deposition (figure 10), where truncations of reflectors against chimney flanks, potential indicators of paleo activity, are observed (Plaza-Faverola et al., subm.)

Acknowledgments

References

Anketell, J.M., Cegla, J., and Dzulynski, S., 1970, On the deformational structures in systems with reversed density gradients: Rocznik Polskiego Towarzystwa Geologicznego, v. 40, p. 3-30.

Berg, K., Solheim, A., and Bryn, P., 2005, The Pleistocene to recent geological development of the Ormen Lange area: Marine and Petroleum Geology, v. 22, p. 45-56.

Berndt, C., 2005, Focused fluid flow in passive continental margins: Philosophical Transactions of the Royal Society a-Mathematical Physical and Engineering Sciences, v. 363, p. 2855-2871.

Berndt, C., Bünz, S., and Mienert, J., 2003, Polygonal fault systems on the mid-Norwegian margin: a long-term source for fluid flow: Subsurface Sediment Mobilization, p. 283-290.

Bertoni, C., and Cartwright, J.A., 2005, 3D seismic analysis of circular evaporite dissolution structures, Eastern Mediterranean: Journal of the Geological Society, v. 162, p. 909.

Bouriak, S., Vanneste, M., and Saoutkine, A., 2000, Inferred gas hydrates and clay diapirs near the Storegga Slide on the southern edge of the Voring Plateau, offshore Norway: Marine Geology, v. 163, p. 125-148.

Brekke, H., 2000, The Tectonic Evolution of the Norwegian Sea Continental Margin with Emphasis on the Vøring and Møre Basins: Dynamics of the Norwegian Margin (ed. by A. Nottvedt, B.T. Larsen, S. Olaussen, B. Torudbakken, J. Skogseid, R.H.Gabrielsen, H. Brekke, O. Birkeland), v. 167, p. 327–378.

Brekke, H., Dahlgren, S., Nyland, B., and Magnus, C., 1999, The prospectivity of the Vøring and Møre basins on the Norwegian Sea continental margin, Geological Society Pub House, p. 261.

Bryn, P., Berg, K., Stoker, M.S., Haflidason, H., and Solheim, A., 2005, Contourites and their relevance for mass wasting along the Mid-Norwegian Margin: Marine and Petroleum Geology, v. 22, p. 85-96.

Bünz, S., and Mienert, J., 2004, Acoustic imaging of gas hydrate and free gas at the Storegga Slide: Journal of Geophysical Research-Solid Earth, v. 109, p. B04102.

Bünz, S., Mienert, J., and Berndt, C., 2003, Geological controls on the Storegga gas-hydrate system of the mid-Norwegian continental margin: Earth and Planetary Science Letters, v. 209, p. 291-307.

Bünz, S., Mienert, J., Vanneste, M., and Andreassen, K., 2005, Gas hydrates at the Storegga Slide: Constraints from an analysis of multicomponent, wide-angle seismic data: Geophysics, v. 70, p. B19-B34.

Bünz, S., Petersen, J., Iversen, S., Chand, S., Bialas, J., Rajan, A., Pless, G., Frantzen, J., Weibull, W., Poluboyarinov, M., Mandal, M., and Tiwari, A., 2008, Gas hydrates and fluid flow vents of the NBS-margin: Nyegga-northern flank of Storegga slide (P-cable 3D seimsic aqcuisition, cruise report). Petromaks-Gans and fluid flow project. Tromsø-Tromsø, 13/07/08-26/07/08, R/V Jan Mayen.

Cartwright, J., Huuse, M., and Aplin, A., 2007, Seal bypass systems: AAPG bulletin, v. 91, p. 1141.

Cathles, L.M., Su, Z., and Chen, D., 2010, The physics of gas chimney and pockmark formation, with implications for assessment of seafloor hazards and gas sequestration: Marine and Petroleum Geology, v. 27, p. 82-91.

Clark, J.I., Chari, T.R., Landva, J., and Woodworth-Lynas, C.M.T., 1989, Pipeline route selection in an iceberg-scoured seabed: Marine Geotechnology, v. 8, p. 51-67.

Dahlgren, K.I.T., Vorren, T.O., and Laberg, J.S., 2002, Late Quaternary glacial development of the mid-Norwegian margin - 65 to 68 degrees N: Marine and Petroleum Geology, v. 19, p. 1089-1113.

Dalland, A., Worsley, D., and Ofstad, K., 1988, A lithostratigraphic scheme for the Mesozoic and Cenozoic succession offshore mid-and northern Norway: Norwegian Petroleum Directorate Bulletin, v. 4, p. 65.

Eidvin, T., Jansen, E., Rundberg, Y., Brekke, H., and Grogan, P., 2000, The upper Cainozoic of the Norwegian continental shelf correlated with the deep sea record of the Norwegian Sea and the North Atlantic: Marine and Petroleum Geology, v. 17, p. 579-600.

Gay, A., and Berndt, C., 2007, Cessation/reactivation of polygonal faulting and effects on fluid flow in the Voring Basin, Norwegian Margin: Journal of the Geological Society, v. 164, p. 129-141.

Gómez, M., and Vergés, J., 2005, Quantifying the contribution of tectonics vs. differential compaction in the development of domes along the Mid-Norwegian Atlantic margin: Basin Research, v. 17, p. 289-310.

Hansen, J.P.V., Cartwright, J.A., Huuse, M., and Clausen, O.R., 2005, 3D seismic expression of fluid migration and mud remobilization on the Gjallar Ridge, offshore mid-Norway: Basin Research, v. 17, p. 123-139.

Hjelstuen, B.O., Eldholm, O., and Skogseid, J., 1999, Cenozoic evolution of the northern Voring margin: Geological Society of America Bulletin, v. 111, p. 1792-1807.

Hjelstuen, B.O., Haflidason, H., Sejrup, H.P., and Nygård, A., 2009, Sedimentary and structural control on pockmark development—evidence from the Nyegga pockmark field, NW European margin: Geo-Marine Letters, p. 1-10.

Hjelstuen, B.O., Sejrup, H.P., Haflidason, H., Nygard, A., Ceramicola, S., and Bryn, P., 2005, Late Cenozoic glacial history and evolution of the Storegga Slide area and adjacent slide flank regions, Norwegian continental margin: Marine and Petroleum Geology, v. 22, p. 57-69.

Hohbein, M., and Cartwright, J., 2006, 3D seismic analysis of the West Shetland Drift system: Implications for Late Neogene palaeoceanography of the NE Atlantic: Marine Geology, v. 230, p. 1-20.

Hornbach, M.J., Saffer, D.M., and Holbrook, W.S., 2004, Critically pressured free-gas reservoirs below gas-hydrate provinces: Nature, v. 427, p. 142-144.

Hovland, M., and Judd, A.G., 1988, Seabed Pockmarks and Seepages. Impact on Geology, Biology and the Marine Environment. Graham & Trotman Ltd., London., 293 p.

Hovland, M., Svensen, H., Forsberg, C.F., Johansen, H., Fichler, C., Fossa, J.H., Jonsson, R., and Rueslatten, H., 2005, Complex pockmarks with carbonate-ridges off mid-Norway: Products of sediment degassing: Marine Geology, v. 218, p. 191-206.

Hustoft, S., Bünz, S., and Mienert, J., 2010, Three-dimensional seismic analysis of the morphology and spatial distribution of chimneys beneath the Nyegga pockmark field, offshore mid-Norway: Basin Research, v. 22, p. 465-480.

Hustoft, S., Dugan, B., and Mienert, J., 2009, Effects of rapid sedimentation on developing the Nyegga pockmark field: Constraints from hydrological modeling and 3-D seismic data, offshore mid-Norway: Geochemistry Geophysics Geosystems, v. 10, p. Q06012.

Hustoft, S., Mienert, J., Bünz, S., and Nouzé, H., 2007, High-resolution 3D-seismic data indicate focussed fluid migration pathways above polygonal fault systems of the mid-Norwegian margin: Marine Geology, v. 245, p. 89-106.

Haacke, R.R., Hyndman, R.D., Park, K.P., Yoo, D.G., Stoian, I., and Schmidt, U., 2009, Migration and venting of deep gases into the ocean through hydrate-choked chimneys offshore Korea: Geology, v. 37, p. 531-534.

Haacke, R.R., Westbrook, G.K., and Hyndman, R.D., 2007, Gas hydrate, fluid flow and free gas: Formation of the bottom-simulating reflector: Earth and Planetary Science Letters, v. 261, p. 407-420.

Haacke, R.R., Westbrook, G.K., and Riley, M.S., 2008, Controls on the formation and stability of gas hydrate-related bottom-simulating reflectors (BSRs): A case study from the west Svalbard continental slope: J. geophys. Res, v. 113.

Imber, J., Holdsworth, R.E., McCaffrey, K.J.W., Wilson, R.W., Jones, R.R., England, R.W., and Gjeldvik, G., 2005, Early Tertiary sinistral transpression and fault reactivation in the western Voring Basin, Norwegian Sea: Implications for hydrocarbon exploration and pre-breakup deformation in ocean margin basins: AAPG bulletin, v. 89, p. 1043.

Ivanov, M., Westbrook, G.K., Blinova, V., Kozlova, E., Mazzini, A., Nouzé, H., and Minshull, T.A., 2007, First Sampling of Gas Hydrate From the Vøring Plateau: Eos Trans. AGU, v. 88, p. 209.

Jose, T., Minshull, T.A., Westbrook, G.K., Nouzé, H., Ker, S., Gailler, A., Exley, R., and Berndt, C., 2008, A Geophysical Study of a Pockmark in the Nyegga Region, Norwegian Sea. Proceedings of the 6th International Conference on Gas Hydrates (ICGH 2008), Vancouver, British Columbia, CANADA, July 6-10, 2008, 12pp. [https://circle.ubc.ca/handle/2429/1022].

Judd, A.G., and Hovland, M., 2007, Seabed fluid flow: the impact of geology, biology and the marine environment., Cambridge University Press, Cambridge, 475 p.

Judd, A.G., Sim, R., Kingston, P., and McNally, J., 2002, Gas seepage on an intertidal site: Torry Bay, Firth of Forth, Scotland: Continental Shelf Research, v. 22, p. 2317-2331.

Kjeldstad, A., Skogseid, J., Langtangen, H.P., Bjorlykke, K., and Hoeg, K., 2003, Differential loading by prograding sedimentary wedges on continental margins: An arch-forming mechanism: Journal of Geophysical Research-Solid Earth, v. 108, p. NO. B1, 2036.

Kvenvolden, K.A., and Barnard, L.A., 1983, Hydrates of natural gas in continental margins: Studies in Continental Margin Geology, v. 34, p. 631-640.

Leynaud, D., Mienert, J., and Vanneste, M., 2009, Submarine mass movements on glaciated and non-glaciated European continental margins: A review of triggering mechanisms and preconditions to failure: Marine and Petroleum Geology, v. 26, p. 618-632.

Liu, X.L., and Flemings, P.B., 2007, Dynamic multiphase flow model of hydrate formation in marine sediments: Journal of Geophysical Research-Solid Earth, v. 112, p. B03101.

Lundin, E., and Doré, A.G., 2002, Mid-Cenozoic post-breakup deformation in the [] passive'margins bordering the Norwegian-Greenland Sea: Marine and Petroleum Geology, v. 19, p. 79-93.

Løseth, H., Gading, M., and Wensaas, L., 2009, Hydrocarbon leakage interpreted on seismic data: Marine and Petroleum Geology, v. 26, p. 1304-1319.

Løseth, H., Wensaas, L., Arntsen, B., and Hovland, M., 2003, Gas and fluid injection triggering shallow mud mobilization in the Hordaland Group, North Sea: Geological Society London Special Publications, v. 216, p. 139.

Mazzini, A., Svensen, H., Hovland, M., and Planke, S., 2006, Comparison and implications from strikingly different authigenic carbonates in a Nyegga complex pockmark, G11, Norwegian Sea: Marine Geology, v. 231, p. 89-102.

Mienert, J., Andreassen, K., Posewang, J., and Lukas, D., 2000, Changes of the hydrate stability zone of the Norwegian margin from glacial to interglacial times: Gas Hydrates: Challenges for the Future, v. 912, p. 200-210.

Mienert, J., Bünz, S., Guidard, S., Vanneste, M., and Berndt, C., 2005a, Ocean bottom seismometer investigations in the Ormen Lange area offshore mid-Norway provide evidence for shallow gas layers in subsurface sediments: Marine and Petroleum Geology, v. 22, p. 287-297.

Mienert, J., and Posewang, J., 1999, Evidence of shallow- and deep-water gas hydrate destabilizations in North Atlantic polar continental margin sediments: Geo-Marine Letters, v. 19, p. 143-149.

Mienert, J., Posewang, J., and Baumann, M., 1998, Gas hydrates along the north-eastern Atlantic Margin: possible hydrate bound margin instabilities and possible release of methane, in: Henriet, J.-P., Mienert, J. (Eds.), Gas Hydrates: Relevance to World Margin Stability and Climatic Change: Geological Society of London, Special Publication v. 137, p. 275-291.

Mienert, J., Vanneste, M., Bünz, S., Andreassen, K., Haflidason, H., and Sejrup, H.P., 2005b, Ocean warming and gas hydrate stability on the mid-Norwegian margin at the Storegga Slide: Marine and Petroleum Geology, v. 22, p. 233-244.

Minshull, T., and White, R., 1989, Sediment compaction and fluid migration in the Makran accretionary prism: J. geophys. Res, v. 94, p. 7387–7402.

Nimblett, J., and Ruppel, C., 2003, Permeability evolution during the formation of gas hydrates in marine sediments: J. geophys. Res, v. 108, p. 2–1.

Nouzé, H., and Fabri, M.-C., et l'équipe scientifique embarquée, 2007, Vicking cruise report –Cold Seeps on the Norwegian Margin. Associated Ecosystem – R/V Pourquoi pas ? May 19th – June 18th, 2006. Alesund- Alesund. Report no. GM/07- 02, Ifremer, Département des Géosciences Marines, Ifremer.

Nygård, A., Sejrup, H.P., Haflidason, H., and Bryn, P., 2005, The glacial North Sea Fan, southern Norwegian Margin: architecture and evolution from the upper continental slope to the deep-sea basin: Marine and Petroleum Geology, v. 22, p. 71-84.

Paull, C.K., Ussler, W., Holbrook, W.S., Hill, T.M., Keaten, R., Mienert, J., Haflidason, H., Johnson, J.E., Winters, W.J., and Lorenson, T.D., 2008, Origin of pockmarks and chimney structures on the flanks of the Storegga Slide, offshore Norway: Geo-Marine Letters, v. 28, p. 43-51.

Petersen, C.J., Bünz, S., Hustoft, S., Mienert, J., and Klaeschen, D., 2010, High-resolution P-Cable 3D seismic imaging of gas chimney structures in gas hydrated sediments of an Arctic sediment drift: Marine and Petroleum Geology, v. doi: 10.1016/j.marpetgeo.2010.06.006, p. 1-14.

Pilcher, R., and Argent, J., 2007, Mega-pockmarks and linear pockmark trains on the West African continental margin: Marine Geology, v. 244, p. 15-32.

Plaza-Faverola, A., Bünz, S., and Mienert, J., 2010a, Fluid distributions inferred from P-wave velocity and reflection seismic amplitude anomalies beneath the Nyegga pockmark field of the mid-Norwegian margin: Marine and Petroleum Geology, v. 27, p. 46-60.

Plaza-Faverola, A., Westbrook, G.K., Ker, S., Exley, R., Gailler, A., Minshull, T.A., and Broto, K., 2010b, Evidence from 3D seismic tomography for a substantial accumulation of gas hydrate in a fluid-escape chimney in the Nyegga pockmark field, offshore Norway: J. Geophys. Res, v. doi:10.1029/2009JB007078, in press.

Reemst, P., Skogseid, J., and Larsen, B.T., 1996, Base Pliocene velocity inversion on the eastern Voring Margin - Causes and implications: Global and Planetary Change, v. 12, p. 201-211.

Riedel, M., Novosel, I., Spence, G.D., Hyndman, R.D., Chapman, R.N., Solem, R.C., and Lewis, T., 2006, Geophysical and geochemical signatures associated with gas hydrate-related venting in the northern Cascadia margin: Geological Society of America Bulletin, v. 118, p. 23-38.

Riis, F., Berg, K., Cartwright, J., Eidvin, T., and Hansch, K., 2005, Formation of large, crater-like evacuation structures in ooze sediments in the Norwegian Sea. Possible implications for the development of the Storegga Slide: Marine and Petroleum Geology, v. 22, p. 257-273.

Rise, L., Ottesen, D., Longva, O., Solheim, A., Andersen, E.S., and Ayers, S., 2006, The Sklinnadjupet slide and its relation to the Elsterian glaciation on the mid-Norwegian margin: Marine and Petroleum Geology, v. 23, p. 569-583.

Sejrup, H.P., Larsen, E., Landvik, J., King, E.L., Haflidason, H., and Nesje, A., 2000, Quaternary glaciations in southern Fennoscandia: evidence from southwestern Norway and the northern North Sea region: Quaternary Science Reviews, v. 19, p. 667-685.

Skogseid, J., Pedersen, T., Eldholm, O., and Larsen, B.T., 1992, Tectonism and magmatism during NE Atlantic continental break-up: the Voring Margin: Geological Society London Special Publications, v. 68, p. 305.

Solheim, A., Berg, K., Forsberg, C.F., and Bryn, P., 2005, The Storegga Slide complex: repetitive large scale sliding with similar cause and development: Marine and Petroleum Geology, v. 22, p. 97-107.

Spencer, A.M., Birkeland, Ø., Knag, G., and Fredsted, R., 1999, Petroleum systems of the Atlantic margin of northwest Europe, Volume 5, Geological Society of London, p. 231.

Stoker, M.S., Praeg, D., Hjelstuen, B.O., Laberg, J.S., Nielsen, T., and Shannon, P.M., 2005, Neogene stratigraphy and the sedimentary and oceanographic development of the NW European Atlantic margin: Marine and Petroleum Geology, v. 22, p. 977-1005.

Tjelta, T., Svan, G., Strout, J., Forsberg, C., Planke, S., and Johansen, H., 2007, Gas Seepage and Pressure Buildup at a North Sea Platform Location: Gas Origin, Transport Mechanisms, and Potential Hazards.

Van Bemmel, P.P., and Pepper, R.E.F., 2000, Seismic signal processing method and apparatus for generating a cube of variance values, Google Patents.

Vanneste, M., and Mienert, J., 2005, DYNAMICS OF GAS HYDRATE RE-EQUILIBRATION: EXAMPLES FROM THE NATURAL ENVIRONMENT: Proceedings of the Fifth International Conference on Gas Hydrates, June 12-16, 2005. Trondheim, Norway.

Vaular, E.N., Barth, T., and Haflidason, H., 2010, The geochemical characteristics of the hydrate-bound gases from the Nyegga pockmark field, Norwegian Sea: Organic Geochemistry, In press.

Westbrook, G.K., Chand, S., Rossi, G., Long, C., Bünz, S., Camerlenghi, A., Carcione, J.M., Dean, S., Foucher, J.P., Flueh, E., Gei, D., Haacke, R.R., Madrussani, G., Mienert, J., Minshull, T.A., Nouzé, H., Peacock, S., Reston, T.J., Vanneste, M., and Zillmer, M., 2008a, Estimation of gas hydrate concentration from multi-component seismic data at sites on the continental margins of NW Svalbard and the Storegga region of Norway: Marine and Petroleum Geology, v. 25, p. 744-758.

Westbrook, G.K., Exley, R., Minshull, T.A., Nouzé, H., Gailler, A., Jose, T., Ker, S., and Plaza, A., 2008b, High-resolution 3D seismic investigations of hydrate-bearing fluid-escape chimneys in the Nyegga region of the Vøring plateau, Norway, Proceedings of the 6th International Conference on Gas Hydrates (ICGH 2008), Vancouver, British Columbia, CANADA, July 6-10, 2008, 12pp. [https://circle.ubc.ca/handle/2429/1022].
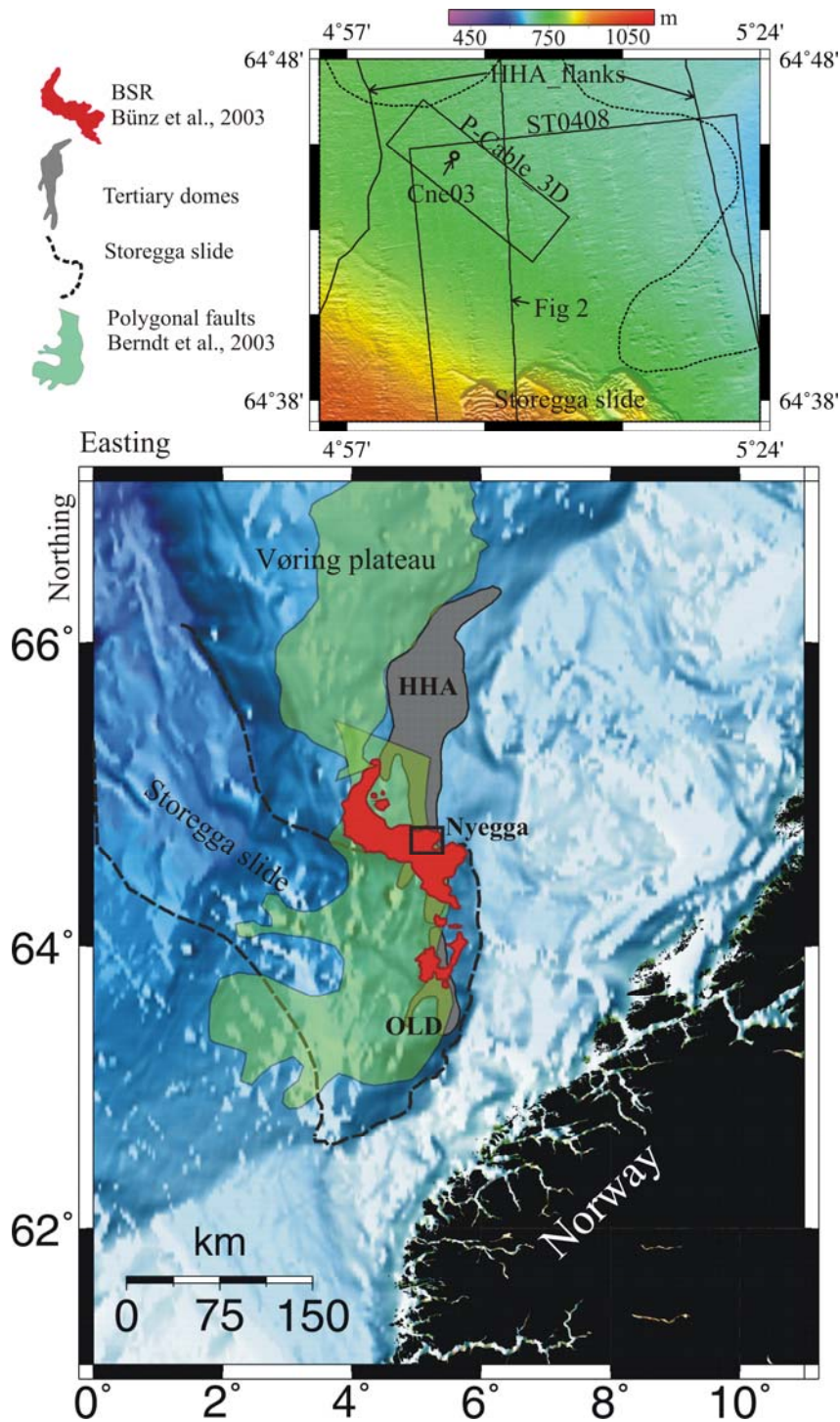
Figure 1: Location map showing the position of the Nyegga area at the mid-Norwegian continental margin and respect to the Storegga slide (dashed line). Two of the more prominent Tertiary domes are included: the Helland Hansen Arch (HHA) and the Ormen Lange Dome (OLD). BSR (Bünz et al., 2003) and polygonal faults (Berndt et al., 2003) maps in the region are projected. The inset shows water depth range in the study area (650-900 m) and coverage of the P-Cable 3D and the ST0408 seismic data sets.
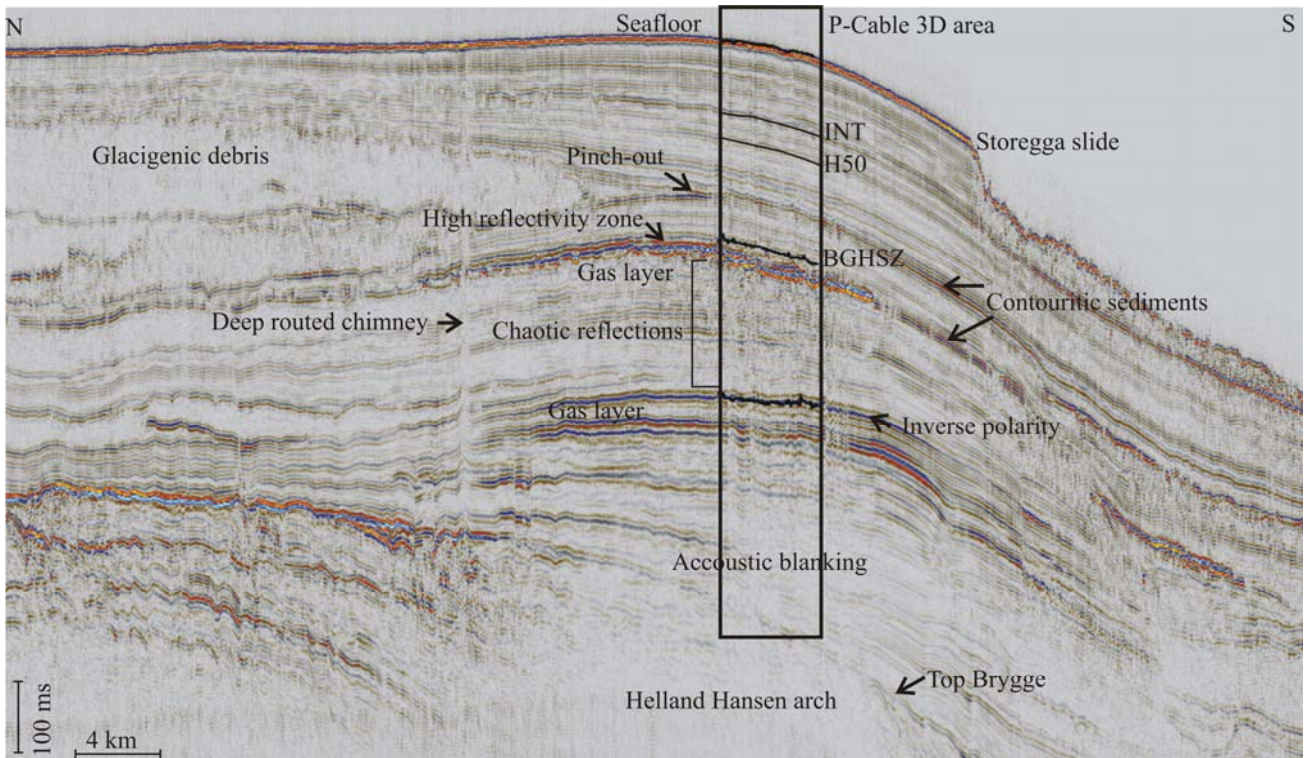
Figure 2: Regional 2D seismic section integrating geophysical and geological settings relevant for the investigation of the gas hydrate system in Nyegga. This study concentrates on the high-resolution P-cable 3D seismic located between the northern side wall of the Storegga slide and the front of glacigenic debris flow pinching out at the northern flank of the Helland Hansen Arch. The base of the gas hydrate stability zone (BGHSZ) and other stratigraphical levels are projected as reference.
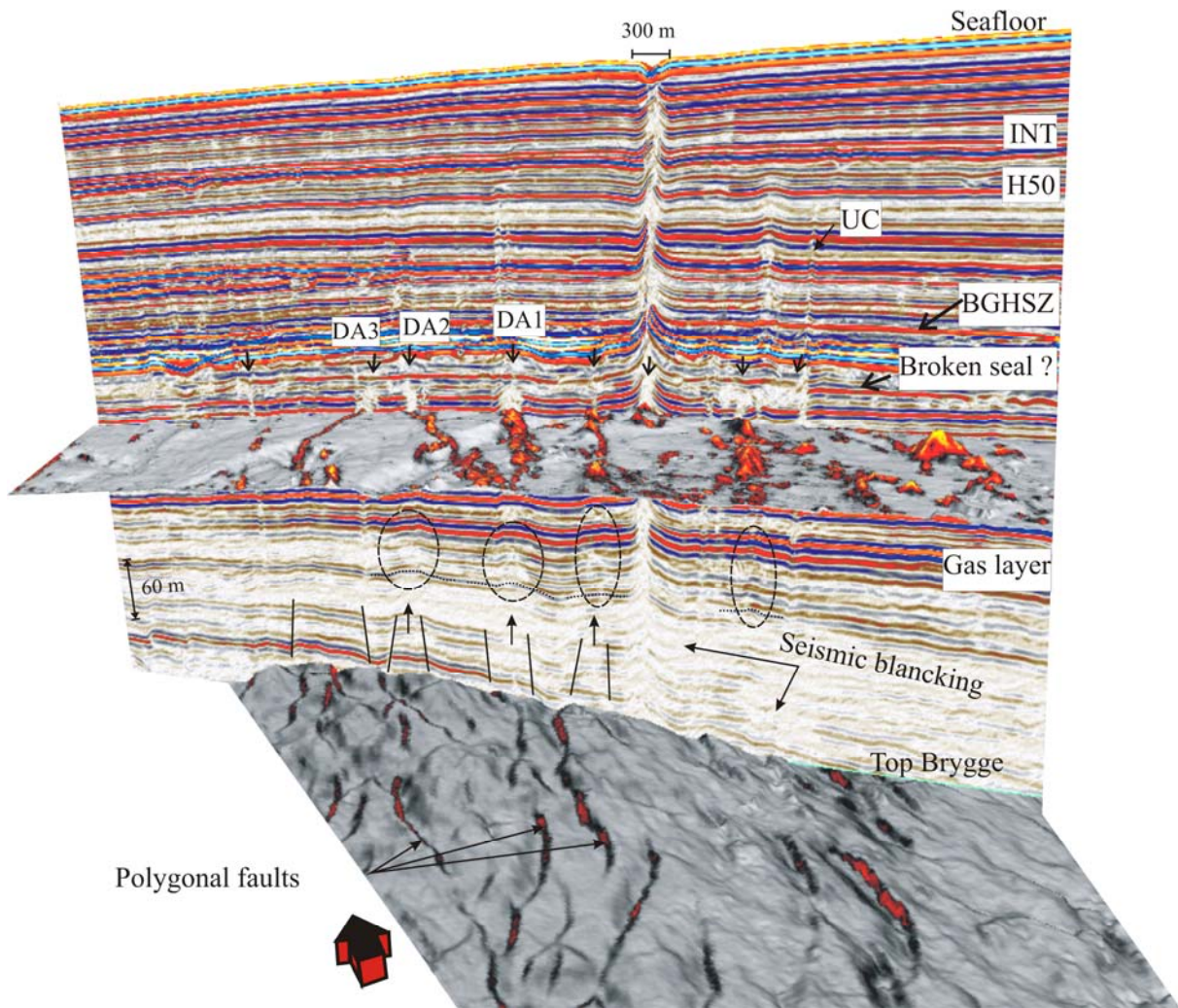
Figure 3: Vertical seismic section from the P-Cable 3D data set showing the seismic character of the chaotic, dim amplitude lineations (indicated by vertical arrows) within the present day gas layer beneath the GHSZ and its location respect to the faults mapped at the top of the Brygge formation (ST0408 data set). Three of the dimming anomalies (DA1-3) are zoomed in (figure 4). The shallower variance map corresponds to map C in figure 5. Sets of polygonal faults with opposite dips get closer to each other at the base of the dim amplitude anomalies. Sediments between the chaotic anomalies and the deeper faults are upward bended (dashed lines). UC stands for "Unit chimney".

Figure 4: Interpretation of interrupted reflectors at the location of three of the observed dim amplitude anomalies (DA1, DA2, DA3). An envelope of the anomalies (dashed lines) shows the characteristic conical pattern. Faults with opposite dips but progressing towards the base of the anomalies are interpreted. Paleo-BGHSZ2 corresponds to the "Broken seal" reflector indicated in figure 3. Theoretical depths of the BGHSZ (see appendix) take into account assumptions about changes in eustatic sea-level (Dahlgren et al., 2002), sedimentation rate (Hjelstuen et al., 2005) and sediment interval thicknesses from Vp models (Plaza-Faverola et al., 2010b), subsidence rate (Dahlgren et al., 2002; Hjelstuen et al., 2005) and ocean temperature (Mienert and Posewang, 1999; Mienert et al. 2002; Vanneste and Mienert, 2005). The local theoretical base GHSZ was calculated for the present day using the same assumptions and curves used by Plaza-Faverola et al., 2010b.
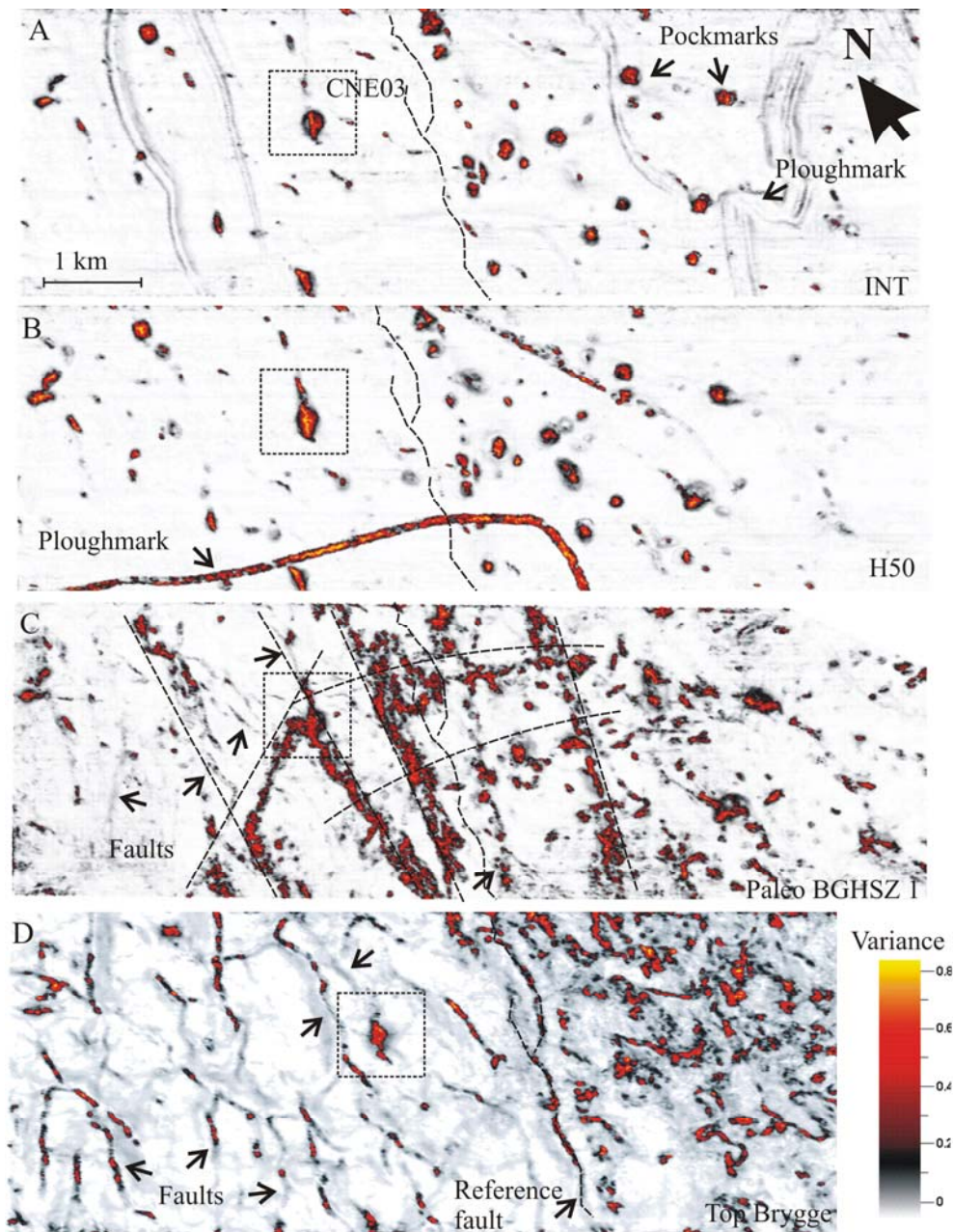
Figure 5: Variance maps from the P-Cable 3D data set enhancing chimneys, dim amplitude anomalies and faults at different stratigraphical levels (see figure 3 for maps' depths). The highest variance values (lighter) indicate strong lateral amplitude discontinuities. From bottom to top the maps represent: (D) faults at the top Brygge formation; (C) dim amplitude anomalies showing lineations in a polygonal pattern (dashed lines) at the depth of an interrupted reflector beneath the present-day BGHSZ (see figure 4); (B) and (A) pockmarks and iceberg ploughmarks at the H50 and INT reflectors respectively. The reference fault at the top of Brygge (D) is projected at shallower horizons to facilitate comparison of the orientation of the different features.
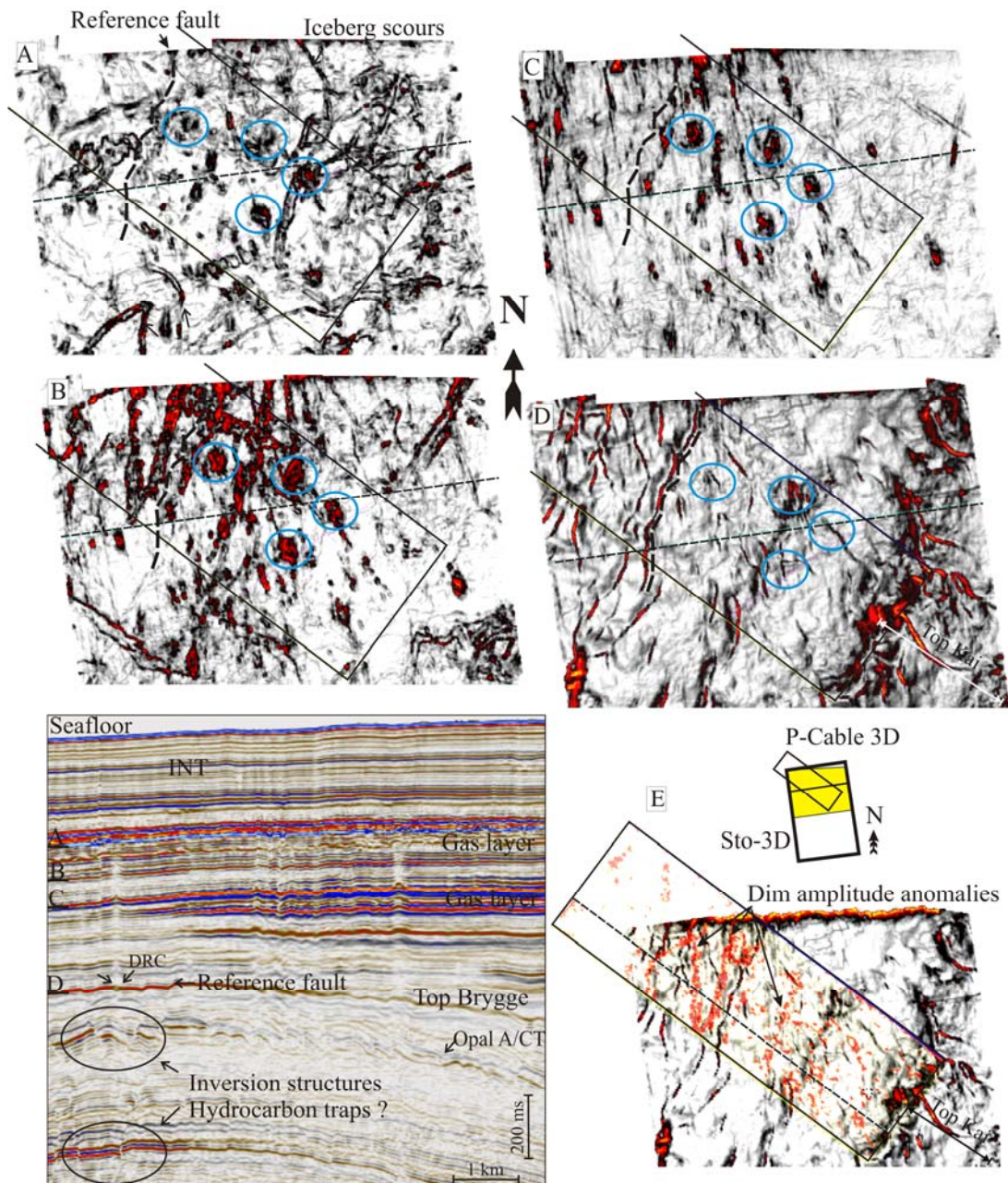
Figure 6: Consecutive Variance maps (A-D) from the ST0408 data set showing lateral amplitude discontinuities at different depth (A-D in the seismic profile) between the present day base GHSZ and the top of Brygge formation. Map E is the same variance map in D but with the high resolution variance map with din amplitude anomalies superimposed, showing that the dimming pattern follows the faults orientation. Warm colors indicate high variance. DRC stands for "deep routed chimney". The reference fault is projected at the different depths. For comparison of faults orientation with figure 5 notice that figure 5 shows north rotated counter clockwise.
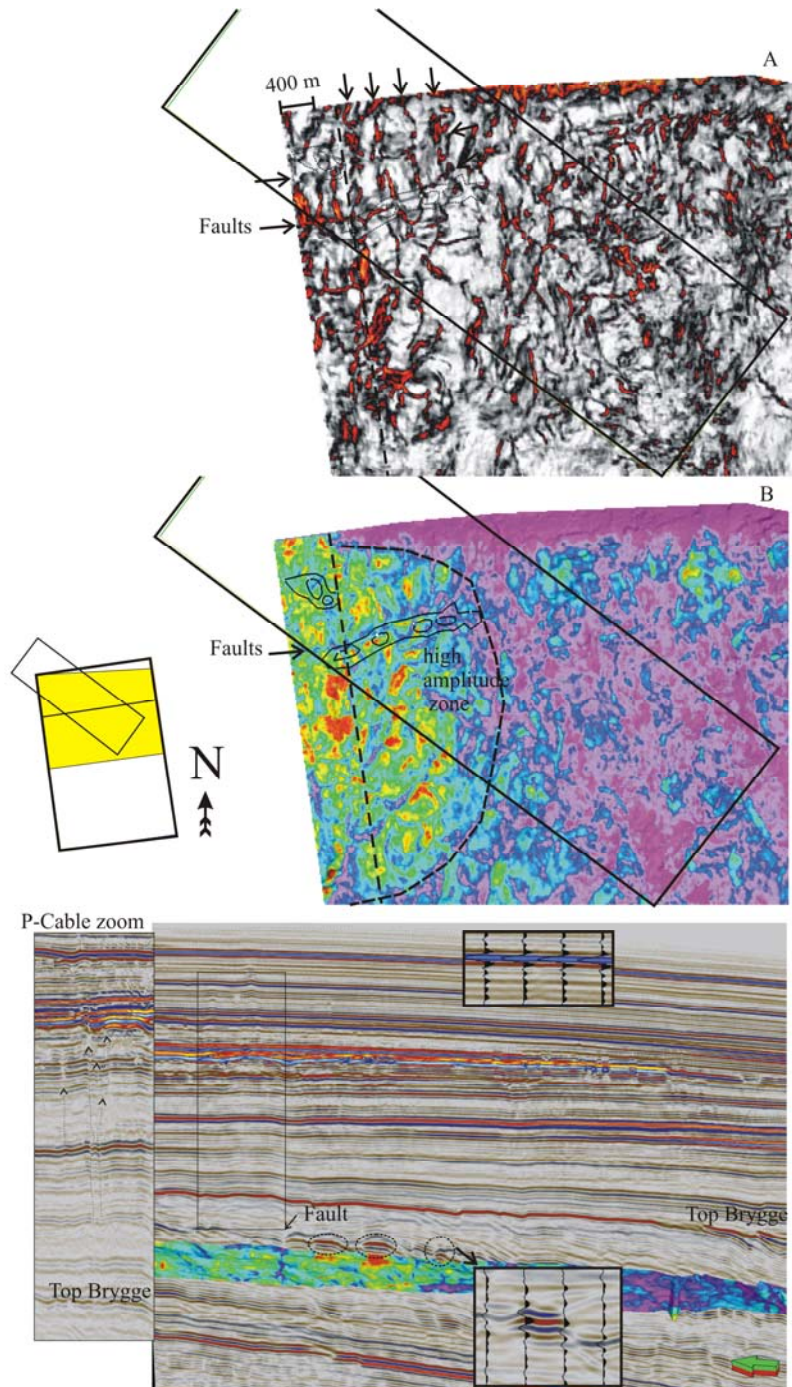
28

Figure 7: Variance (A) and RMS (B) maps from the ST0408 data set at the top of tilted blocks beneath the top of Brygge. Orthogonal faults form blocks of about 400 x 700 m dimensions. The fault pattern differs from the one at the top of Brygge (compare with figure 6). A high amplitude zone conformed by phase reversal bright spots is evidenced in the RMS map (B).
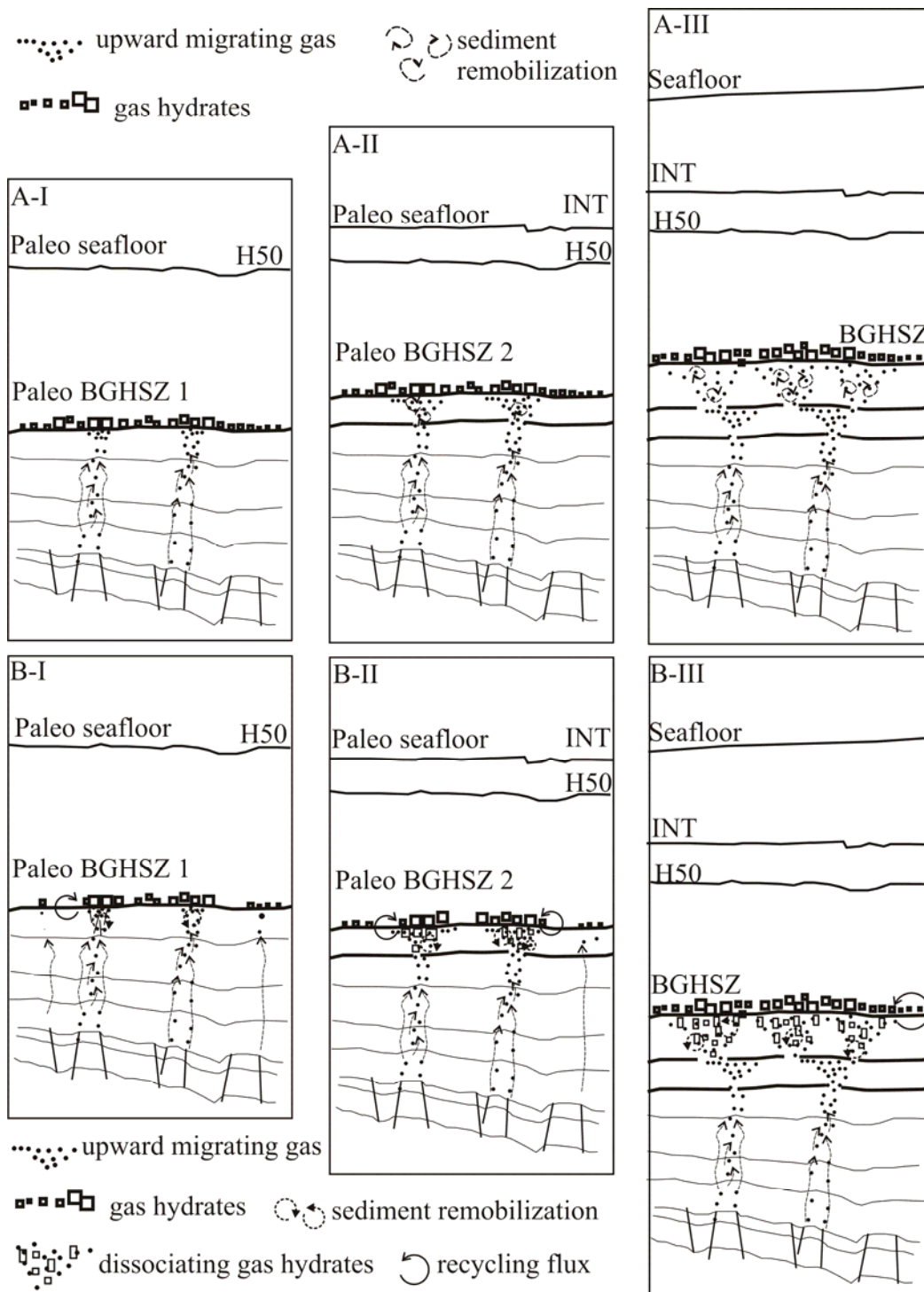
Figure 8: Inferred model of sediment remobilization at the gas-sediment contact beneath GHSZs explaining dim amplitude anomalies observed in the seismic. AI-III inferred model where sediment structure is broken only by buoyant fluid. BI-III inferred model where sediment remobilization is induced by gas hydrate disintegration and further invasion of empty space by buoyant fluids. Three stages of progression of the BGHSZ since first emplacement till present are envisaged (I-III).
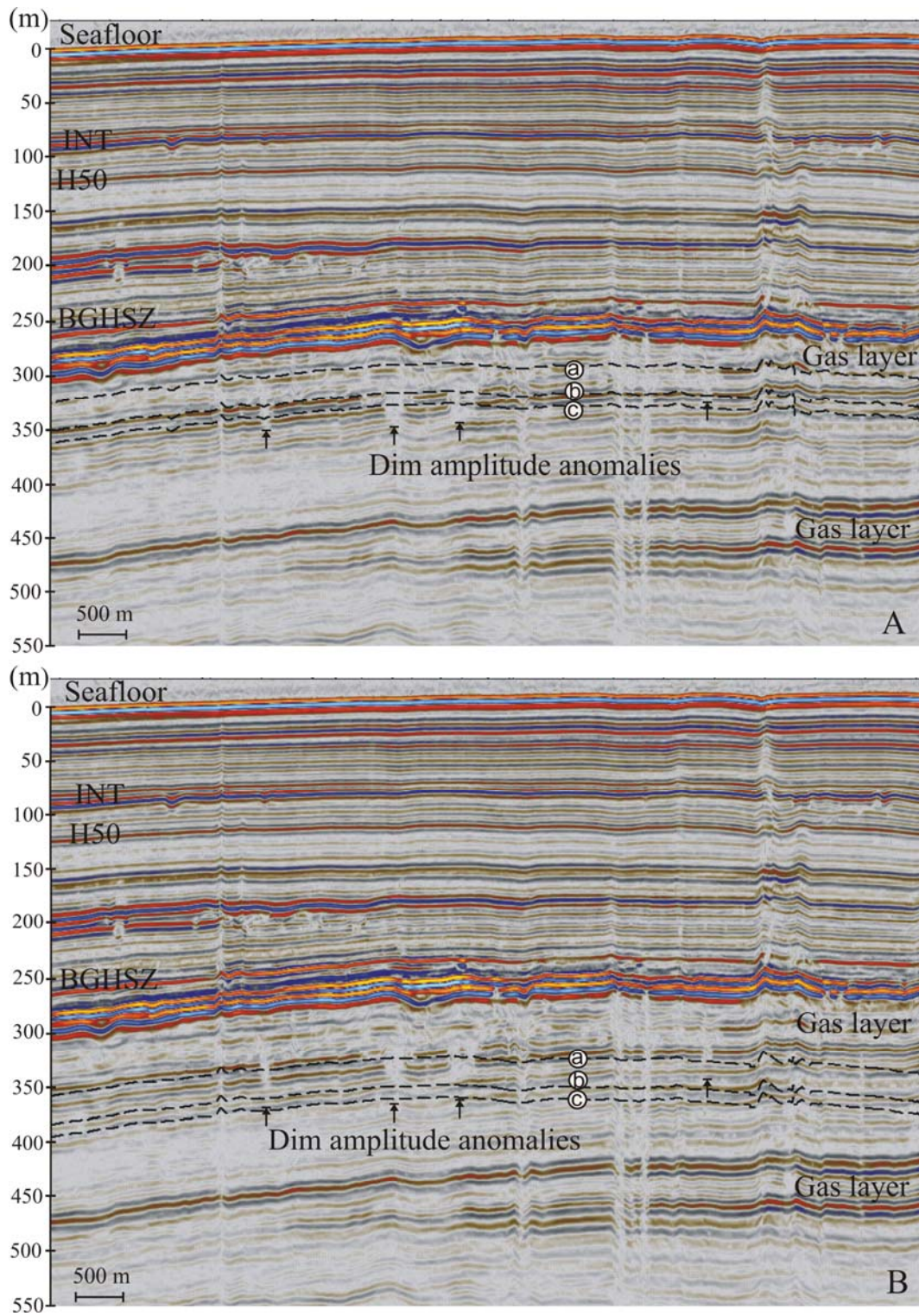
Figure 9: Projection of estimated paleo BGHSZ (dashed lines) on the seismic section at the time of deposition of INT (A) and H50 (B). The three displayed estimated depth bases (a, b, c) correspond to extreme subsidence rates scenarios (appendix A, figure A1).
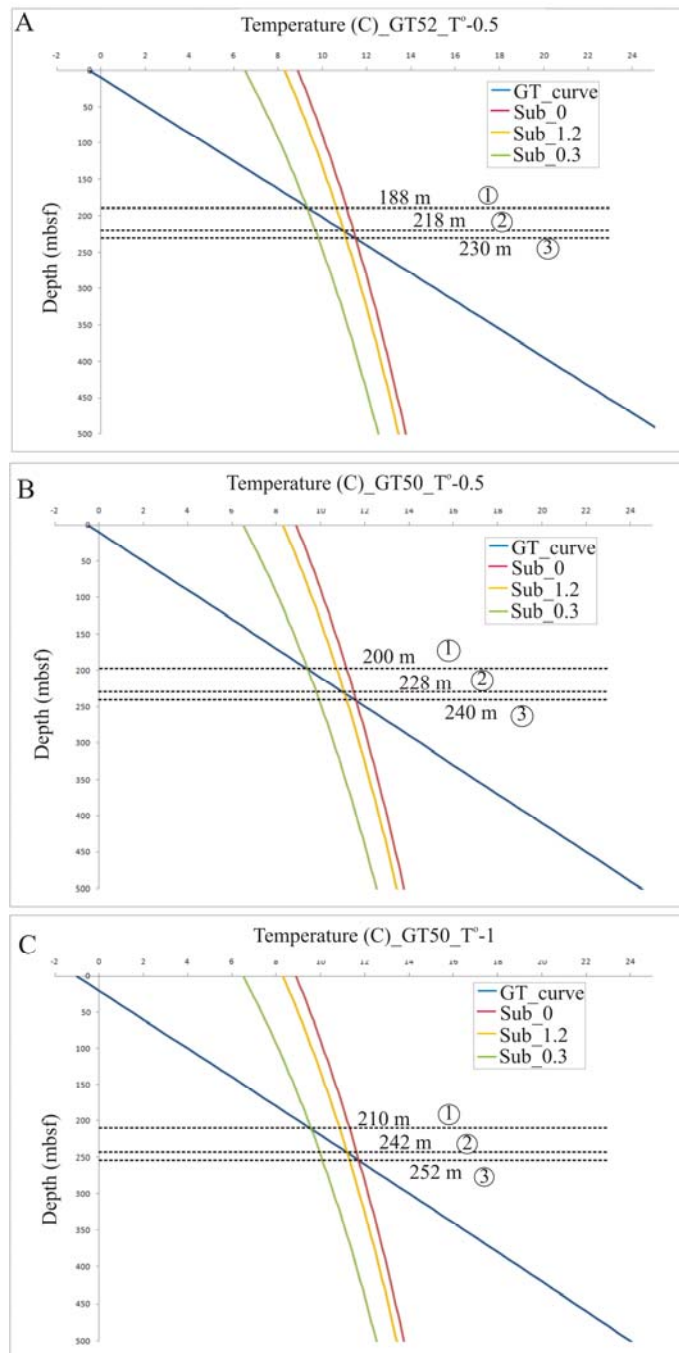
Figure A-1: Hydrate stability curves for a sea-level 100 m lower than the present sea-level at the location of the CNE03 chimney in Nyegga. Three curves are considered, for subsidence rates of: (1) 1.2 m/ka (Dahlgren et al., 2002); (2) 0.3 m/ka (Hjelstuen et al., 2005); and (3) 0. Depths of BGHSZs were estimated for three temperature curves: (A) GT(geothermal gradient)=52 C°/km and T_o(initial temperature)=-0,5 C°; (B) GT=50 C°/km and T_o=-0,5 C°; (C) GT=50 C°/km and T_o=-1 C°.

Event	Chronology based on publications		
Naust T	0-0.2 My (Rise et al., 2006)		
Storegga slide	0.008 My (Holocene) (Solheim et al., 2005)		
Youngest pockmarks	0.025 My (Weichelian) (Hustoft et al., 2009)		
Last glaciation (maximum)	0.02 My (Late Weichelian) (Sejrup et al., 2000)		0.02-2.8 My Glacial interglacial sedimentation (Rise et al., 2005)
INT	~0.13 My (Solheim et al., 2005) NE-SW oriented Iceberg ploughmarks (P-cable, INT)		
Naust S	0.2-0.4 My (Rise et al., 2006)	0.15-1.7 My Seven large pre-Holocene slides (Solheim et al., 2005)	
Naust U	NW-SE oriented Iceberg ploughmarks (P-Cable, BGHSZ) 0.4-0.6 My (Rise et al., 2006). Solheim et al., 2005 and Rise 2005 classify it as 0.38-1.1, making a much larger Naust U compared to Rise et al., 2006.		
Naust A	0.6-1.5 My (Rise et al., 2006)		
First ice-stream to the shell	~1.1 My (Serjup et al., 2000)		
Naust N	1.5-2.8 My (Rise et al., 2006)		
Kai	> 2.8 My E.Miocene-L.Pliocene (Solheim et al., 2005)	Polygonal faults (Gay and Berndt, 2007)	
Brygge	Eoc-E. Mioc (Solheim et al, 2005) Cenozoic compresive structures (sto 3d Seismic)		
HHA growing period	Oligocene-Miocene. Tectonic (33-9 My) + differential compaction (9-1.9 My) (Gómez and Vergés, 2005)		
Continental break-up	Eocene (~55 My) (Skogseid et al., 1992)		
Vøring Transpression	L. Paleocen-E.Eocene (Imber et al., 2005)		
Reverse displacement	Upper Cretaceous strata: WNW flank of Helland Hansen Arch (Gómez and Vergés, 2005). Reactivation of Mesozoic faults (Brekke, 2000)		
Consecutive rifting episodes forming the Mid-Norwegian margin.	Permian-Paleocen (Brekke, 2000)		

Table 1: Chronology of major stratigraphical and structural events based on literature. Some of the geological features characterizing the region are indicated in figure 2.

	P-Cable 3D	ST0408	2D_jm2002
Area (km2)	30	350	---
Dominant Frequency (Hz.)	80	60	80
Vertical resolution (m)	~4,6	~6,2	~5
Fresnel zone (m)	---	---	~160
Sampling interval (ms)	1	4	0,4
Bin size (m)	6x6	25x25	---

Table 2: Parameters of acquisition and processing of the P-Cable and ST0408 data sets. The vertical resolutions are taken as $\lambda/4$. Wavelength (λ) was calculated using a water velocity of 1475 m/s. The resolution of the surveys varies according to the purposes of acquisition and processing of the data.